Phase-dependent multiple Andreev reflections in SNS interferometers

J. Lantz,[1] V. S. Shumeiko,[1] E. Bratus,[2] and G. Wendin[1]
[1]*Department of Microelectronics and Nanoscience, Chalmers University of Technology and Göteborg University, S-41296 Göteborg, Sweden*
[2]*Verkin Institute for Low Temperature Physics and Engineering, 310164 Kharkov, Ukraine*
(Received 1 October 2001; published 27 March 2002)

A theory of coherent multiple Andreev reflections (MAR) is developed for superconductor–normal-metal–superconductor interferometers. We consider a Y-shaped normal-electron-beam splitter connecting two superconducting reservoirs, where the two connection points to the same superconductor can have different phases. The current is calculated in the quantum transport regime as a function of applied voltage and phase difference, $I(V,\phi)$. MAR in interferometers incorporate two features: interference in the arms of the splitter, and interplay with Andreev resonances. The latter feature yields enhancement of the subgap current and current peaks with phase-dependent positions and magnitudes. The interference effect leads to suppression of the subgap current and complete disappearance of the current peaks at $\phi=\pi$. The excess current at large voltage decreases and changes sign with increasing phase difference.

DOI: 10.1103/PhysRevB.65.134523 PACS number(s): 74.80.Fp, 74.50.+r, 74.20.Fg

I. INTRODUCTION

Mesoscopic circuits with multiterminal electron wave guides have interesting and useful physical properties. Figure 1 shows an example of a circuit where a Y-branch wave guide acts as a coherent beam splitter for electrons injected from a normal or superconducting reservoir. Such a circuit with normal-electron reservoirs (NYN) has been first suggested to test statistical properties of the Fermi electrons by measuring current-current correlations in the arms of the splitter.[1,2] This correlation is negative for the case of Fermi statistics, which was indeed observed in the experiment.[3] However, the correlations may change the sign and become positive (similar to the case of Bose particles) when the electrons are injected from a superconducting reservoir (NYS).[4] This effect is related to the Cooper pairing in the superconductor.

Another kind of interference effect, namely, a phase-dependent conductance, has been predicted[5,6] for a circuit geometry (SYN) where the arms of the electron-beam splitter are connected to a superconductor. In this case, the electrons undergo Andreev reflection from the normal–metal–superconductor (NS) interfaces,[7] picking up the superconducting phase at the connection points. The phase difference at the connection points is created by a supercurrent flowing along the surface of the superconducting electrode, e.g., due to a presence of a magnetic field (see Fig. 1). The phase dependence of the conductance of such NS interferometers has been observed in a large number of experiments.[8–10]

In this paper, we investigate the properties of current-voltage characteristics of superconductor–normal-metal– superconductor(SNS) interferometers, i.e., SYS circuits where the arms of the Y-branch splitter and the injection lead are connected to superconducting electrodes, as shown in Fig. 1. As is well known, the current between two superconductors at applied voltage $eV<2\Delta$ (Δ is the superconducting gap) is governed by the mechanism of multiple Andreev reflections (MAR's).[11] The fingerprint of this transport mechanism is the subharmonic gap structure (SGS) at $eV=2\Delta/n$.[12,13] In SNS interferometers one should expect the SGS to be significantly modified and become sensitive to the superconducting phase difference (see Fig. 1). This conclusion is supported by the following qualitative argument. One may consider the interferometer as an SNS junction (S_1NS_2) which is coupled to the injection electrode S_3 via the Y-branch wave guide. The SNS junction contains bound Andreev levels which are broadened due to the open connection to the injection lead. The Andreev levels, the energy of which depends on the superconducting phase difference, produce resonances in the current transport between the superconducting reservoirs. These resonances will significantly modify the SGS, similar to the effect of superconducting bound states in long SNS junctions.[14] However, in the SNS interferometers the resonance structures will be phase dependent.[15]

The problem has become particularly interesting due to recent experiments on a three-terminal SNS interferometer

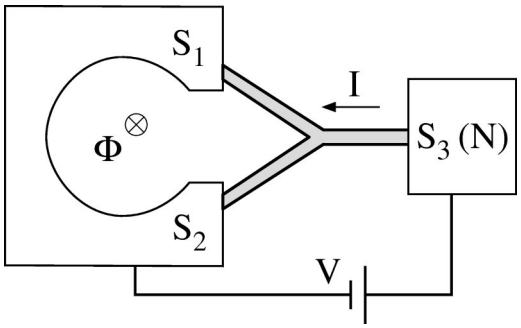

FIG. 1. Schematic picture of the SNS interferometer, which consists of the superconducting loop, to the left, with two electrodes S_1 and S_2 that are connected via the Y-branch wave guide to the right injection electrode S_3, which can be superconducting or normal. The two left electrodes in the loop and the Y-branch wave guide constitute an SNS junction (S_1NS_2), with bound Andreev states broadened due to the coupling to the injection electrode S_3. The phase difference over the S_1NS_2 junction is controlled by means of the magnetic flux through the loop.

by Kutchinsky *et al.*,[16] in which phase dependence of the conductance structures has been observed. In this experiment, the normal region of the interferometer was fabricated with diffusive two-dimensional (2D) metallic film. The effect will be more pronounced with a ballistic normal region, especially in the quantum transport regime, when the Y-wave guide supports a small amount of conducting modes. In practice, such devices could be fabricated with an etched or gated ballistic 2D electron gas in a multilayered semiconducting structure.[17] Quantum transport in NS interferometers has been investigated in Refs. 18–20, and the resonance enhancement of the two-particle Andreev current has been discussed. In SNS interferometers the situation is more complex, since the interplay between the Andreev bound states and MAR's will lead to resonances appearing in all multiparticle currents. The purpose of our study is to develop a MAR theory for SNS interferometers, i.e., to include the interference effect and the effect of Andreev resonances in the MAR calculation scheme[23] and to analyze the phase-dependent current-voltage characteristics (IVC's).

The paper is structured as follows. In Sec. II we present the model of the interferometer and derive equations for the MAR scattering amplitudes. In Sec. III, we present the results of numerical calculation of the IVC's of the interferometer, and in Sec. IV, we present an analytical perturbative analysis of the resonant current structures in the IVC's.

II. SCATTERING STATES

We consider the SNS interferometer shown in Fig. 1, which consists of a normal-electron Y-branch quantum wire, fabricated, e.g., with an etched or gated 2D electron gas, which is connected to two bulk superconducting electrodes. The superconducting electrode connected to the two arms of the splitter is ring shaped, so that magnetic flux can be sent through the ring to induce a superconducting phase difference ϕ between the connection points S_1 and S_2. The current is sent through the interferometer by applying voltage V between the electrode S_3 and the ring.

Our aim is to calculate the injected current as a function of the applied voltage and the phase difference, $I(V,\phi)$. To this end we shall apply the theory of coherent MAR's, which is based on the calculation of scattering states created by incoming quasiparticles from the three superconducting terminals.[13,21–23] For the sake of simplicity, we adopt a single-mode description of the wires and model the splitter by a 3×3 scattering matrix $\hat{S}$ [see Eq. (9) below].

Solving a coherent MAR problem includes the following steps: First the recurrence for the scattering amplitudes is formulated by employing the boundary conditions at the scatterer and at the NS interfaces. Then a solution for the recurrence can be constructed, from which the current is calculated. In the present case of a three-terminal junction, a standard MAR technique cannot be used directly. To solve this problem we will describe the Andreev reflections from the two interfaces of the interferometer, seen by the injector S_3, as a complex reflection from a single effective interface; by doing this we reduce the three-terminal problem to an equivalent two-terminal problem, on which we can apply the standard MAR technique for a two-terminal junctions developed in Ref. 23. Reflection from the interferometer (left interface) is then represented by a nontrivial transfer matrix that contains information about Andreev states in the interferometer. To more clearly understand the effect of the phase difference on the injection current, we will neglect the length of the normal wires and assume all NS interfaces to be completely transparent. This will remove unnecessary complications due to normal-electron resonances[24] and superconducting resonances[14] associated with the Saint-James–de Gennes bound states.[25] At the same time, the resonant property of the junction as well as the phase sensitivity of the current will persist due to the presence of Andreev states in the interferometer with energy $E=\pm E_a$,

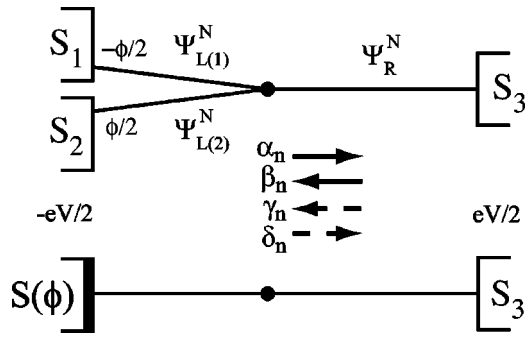

FIG. 2. A close up of the Y-branch wave guide in the SNS interferometer (upper figure) and in the effective two-terminal junction where the left electrode has phase-dependent scattering properties (lower figure). We consider a symmetric phase drop over the SNS junction (the electrodes S_1 and S_2) and a symmetric voltage drop eV from the loop to the injection electrode S_3. The directions of the scattering amplitudes α_n and β_n (for electrons) and γ_n and δ_n (for holes) are shown with arrows.

$$E_a=\Delta\sqrt{1-D\sin^2(\phi/2)}. \tag{1}$$

In the MAR regime, the time-dependent scattering states consist of a superposition of scattered waves with energies $E_n=E+neV$ (n is an integer) shifted with respect to the energy of the incoming wave E. In each branch of the wire the wave functions of the sideband n consists of a superposition of electron and hole plane waves moving in both directions, the corresponding amplitudes being labeled with $\alpha_n,\ldots,\delta_n$ according to Fig. 2. In the normal wires, the scattering state wave function has the form,

$$\Psi^N_{L(i)}=\sum_{n=-\infty}^{\infty}\begin{pmatrix}\alpha_{i,n}e^{ik_n^+x}+\beta_{i,n}e^{-ik_n^+x}\\ \gamma_{i,n}e^{ik_n^-x}+\delta_{i,n}e^{-ik_n^-x}\end{pmatrix}e^{-i[E_n+(eV/2)]t}, \tag{2}$$

$$\Psi^N_R=\sum_{n=-\infty}^{\infty}\begin{pmatrix}\alpha'_ne^{ik_n^+x}+\beta'_ne^{-ik_n^+x}\\ \gamma'_ne^{ik_n^-x}+\delta'_ne^{-ik_n^-x}\end{pmatrix}e^{-i[E_n+(eV/2)]t}, \tag{3}$$

where $\Psi^N_{L(i)}$ is the wave function in the ith wire at the left side ($i=1,2$), x is a coordinate along the wire, Ψ^N_R is the wave function at the right side, and $k_n^\pm=\sqrt{2m(E_F\pm E_n)}$ is

the normal wave vector ($\hbar=1$). In the superconducting electrodes, the corresponding wave functions, including six possible source terms, are

$$\Psi^S_{L(1)}=e^{-i\sigma_z[(eV/2)t-(\phi/4)]}\times\left[(\delta_{1j}\psi_0^+e^{i\tilde{k}_0^+x}+\delta_{2j}\psi_0^-e^{-i\tilde{k}_0^-x})e^{-iEt}+\sum_{-\infty}^{\infty}(A_n\psi_n^+e^{-i\tilde{k}_n^+x}+B_n\psi_n^-e^{i\tilde{k}_n^-x})e^{-iE_nt}\right],$$

$$\Psi^S_{L(2)}=e^{-i\sigma_z[(eV/2)t+(\phi/4)]}\times\left[(\delta_{3j}\psi_0^+e^{i\tilde{k}_0^+x}+\delta_{4j}\psi_0^-e^{-i\tilde{k}_0^-x})e^{-iEt}+\sum_{-\infty}^{\infty}(C_n\psi_n^+e^{-i\tilde{k}_n^+x}+F_n\psi_n^-e^{i\tilde{k}_n^-x})e^{-iE_nt}\right],$$

$$\Psi^S_R=e^{i\sigma_z(eV/2)t}\left[(\delta_{5j}\psi_0^+e^{-i\tilde{k}_0^+x}+\delta_{6j}\psi_0^-e^{i\tilde{k}_0^-x})e^{-iEt}+\sum_{-\infty}^{\infty}(K_n\psi_n^+e^{i\tilde{k}_n^+x}+L_n\psi_n^-e^{-i\tilde{k}_n^-x})e^{-iE_nt}\right], \quad (4)$$

where $A_n,\ldots,L_n$ are constant coefficients and $\psi_n^{\pm}$ are elementary solutions to the Bogoliubov–de Gennes equation[26]

$$\psi_n^{\pm}(E)=\frac{\min(1,\sqrt{\Delta/|E_n|})}{\sqrt{2}}e^{\pm\sigma_z\gamma_n/2}\begin{pmatrix}1\\ \sigma_n\end{pmatrix}, \quad (5)$$

where

$$e^{\gamma_n}=\frac{|E_n|+\xi_n}{\Delta},\quad \xi_n=\begin{cases}\sqrt{E_n^2-\Delta^2} & E_n^2>\Delta^2,\\ i\sigma_n\sqrt{\Delta^2-E_n^2} & E_n^2<\Delta^2,\end{cases}$$

$$\sigma_n=\mathrm{sgn}(E_n),\quad \tilde{k}_n=\sqrt{2m(E_F\pm\xi_n)}, \quad (6)$$

and σ_z is the Pauli matrix. The different source terms are distinguished by the index $j=\{1,2,3,4,5,6\}$ corresponding to injection of an electron/hole from each of the electrodes. Injections from the left and from the right generate essentially different scattering states and currents, and to keep track of the side of injection we will introduce an additional side index $\nu=\mp1$ corresponding to injection from the left electrodes and right electrode, respectively,

$$\nu=-1\Leftrightarrow j\in\{1,2,3,4\},$$

$$\nu=1\Leftrightarrow j\in\{5,6\}. \quad (7)$$

The scattering in the Y-branch splitter is described by a unitary scattering matrix

$$\begin{pmatrix}\beta_{1,n}\\ \beta_{2,n}\\ \alpha_n'\end{pmatrix}=\hat{S}\begin{pmatrix}\alpha_{1,n}\\ \alpha_{2,n}\\ \beta_n'\end{pmatrix}, \quad (8)$$

where the scattering matrix,

$$\hat{S}=\begin{pmatrix}r & d & t\\ d & r & t\\ t & t & r_0\end{pmatrix}, \quad (9)$$

is chosen to be symmetric, $S_{31}=S_{32}=t$, with a real transmission amplitude from right to left, $t>0$, and also to be independent of energy and thus the same for electrons and holes,

$$\begin{pmatrix}\delta_{1,n}\\ \delta_{2,n}\\ \gamma_n'\end{pmatrix}=\hat{S}\begin{pmatrix}\gamma_{1,n}\\ \gamma_{2,n}\\ \delta_n'\end{pmatrix}. \quad (10)$$

The latter approximation is reasonable since the scale of the energy dispersion of the scattering matrix is given by the Fermi energy, while we are interested in a much smaller energy interval comparable to the superconducting gap, $E_F\gg\Delta$. The unitary conditions for $\hat{S}$ are expressed through the equations, $1=R+D+T, 1=|r_0|^2+2T$, where $D=|d|^2, R=|r|^2, T=t^2$, and

$$r_0=-(r+d)^*,\qquad r-d=e^{i\theta'}. \quad (11)$$

The transmission coefficient D concerns the transparency of the SNS junction of the interferometer and controls the position of the Andreev levels, Eq. (1), while the transmission coefficient T describes coupling of the SNS junction to the injection lead.

By means of a canonical transformation the scattering between the injection electrode and the interferometer can be separated from the scattering between the arms of the interferometer. To this end we introduce new scattering amplitudes, $\alpha_n^{\pm}=(\alpha_{1,n}\pm\alpha_{2,n})/\sqrt{2}$, and similarly for β_n,γ_n, and δ_n, and rewrite Eq. (8) in the form

$$\begin{pmatrix}\beta_n^+\\ \alpha_n'\end{pmatrix}=\hat{S}'\begin{pmatrix}\alpha_n^+\\ \beta_n'\end{pmatrix},$$

$$\hat{S}'=\begin{pmatrix}-r_0^* & \sqrt{2T}\\ \sqrt{2T} & r_0\end{pmatrix}, \quad (12)$$

$$\beta_n^-=(r-d)\alpha_n^-. \quad (13)$$

The scattering equations for holes have a similar form. It is clear from Eq. (12) that the transport through the interferometer, from the right electrode to the left electrodes, is independent of the $(-)$ coefficients. Thus, we can treat the junction as an effective two-terminal junction with transparency $2T$.

It is convenient for the further calculations to introduce vector notations,

$$\hat{\alpha}_n^{\pm}=\begin{pmatrix}\alpha_n^{\pm}\\ \beta_n^{\pm}\end{pmatrix}, \quad (14)$$

and similarly for the other scattering amplitudes, and to rewrite Eq. (12) through a transfer matrix

$$\hat{\alpha}_n^+ = \hat{T}\hat{\alpha}_n', \tag{15}$$

where $\hat{T}=(1/\sqrt{2T})(1-|r_0|e^{-i\sigma_z\rho}\sigma_x)$. The same equation also holds for the hole coefficients. It is convenient to gauge out the reflection phase ρ from the transfer matrix, which can be done by a transformation of the scattering amplitudes, $\hat{\alpha}_n^+, \hat{\alpha}_n' \to e^{i\sigma_z\rho/2}\hat{\alpha}_n^+, e^{i\sigma_z\rho/2}\hat{\alpha}_n'$, whereby

$$\hat{T} \to (1/\sqrt{2T})(1-|r_0|\sigma_x). \tag{16}$$

We now proceed with a derivation of the recurrence relation and first consider the right NS interface, where we match the wave functions in Eqs. (3) and (4),

$$\hat{\gamma}_n' = \hat{V}_n^R \hat{\alpha}_{n-1}' + \hat{Y}_j \delta_{1\nu}\delta_{0n}. \tag{17}$$

This is the recurrence relation for an ideal SN interface where the Andreev reflection amplitude is given by

$$\hat{V}_n^R = \sigma_n e^{-\sigma_z\gamma_n}, \tag{18}$$

and the source term,

$$\hat{Y}_j = \frac{\sqrt{2}\xi_0}{\sqrt{|E|}} e^{-\sigma_z\gamma_0/2}\begin{pmatrix} c\,\delta_{j6} \\ \delta_{j5}\end{pmatrix}, \tag{19}$$

corresponds to the injection from the right electrode, $\nu=1$. Similar relations hold for each of the two SN interfaces at the left side. In terms of the vectors $\hat{\alpha}^\pm$ and $\hat{\gamma}^\pm$ introduced in Eq. (14), they have the form

$$\hat{\alpha}_n^+ = \sigma_n e^{-\sigma_z\gamma_n}\left(\hat{\gamma}_{n-1}^+ \cos\frac{\phi}{2} + \hat{\gamma}_{n-1}^- i\sin\frac{\phi}{2}\right), \tag{20}$$

$$\hat{\alpha}_n^- = \sigma_n e^{-\sigma_z\gamma_n}\left(\hat{\gamma}_{n-1}^+ i\sin\frac{\phi}{2} + \hat{\gamma}_{n-1}^- \cos\frac{\phi}{2}\right),$$

for $n\neq 0$. For $n=0$ there is also a source term describing injection from the left electrodes ($\nu=-1$). Now the vectors $\hat{\alpha}^-$ and $\hat{\gamma}^-$ can be eliminated by means of Eq. (13) for electrons and for holes, which yields

$$\hat{\alpha}_n^+ = \hat{V}_n^L \hat{\gamma}_{n-1}^+ + \hat{Y}_j \delta_{-1\nu}\delta_{0n}, \tag{21}$$

where

$$\hat{V}_n^L = \frac{\sigma_n}{\cos\dfrac{\phi}{2}}\left(e^{-\sigma_z\gamma_n} + \sigma_z(\sigma_x e^{i\sigma_z\theta}-1)\frac{\Delta}{2\xi_n}\sin^2\frac{\phi}{2}\right), \tag{22}$$

$\theta=\theta'+\rho$. The source term, Y_j, for $j=1,2$ has the form

$$\hat{Y}_j = \frac{\xi_0}{\sqrt{|E|}} e^{-i\phi/4}\left[e^{-\gamma_0/2}\begin{pmatrix} 1+be^{-\gamma_0} \\ be^{\gamma_0+i\theta}\end{pmatrix} \times \delta_{j1} - e^{\gamma_0/2}\begin{pmatrix} cbe^{-\gamma_0-i\theta} \\ 1+be^{\gamma_0}\end{pmatrix}\delta_{j2}\right], \quad \nu=-1, \tag{23}$$

where $b=i\sigma_0(\Delta/2\xi)\tan(\phi/2)$. The source term for the injection cases $j=3,4$ has a form similar to Eq. (23) with $\phi \to -\phi$.

The matrix $\hat{V}_n^L$ describes complete reflection from the interferometer for energies inside the energy gap, $|E_n|<\Delta$, where it obeys a standard transfer-matrix equation, $\hat{V}_n^L\sigma_z\hat{V}_n^{\dagger L}=\sigma_z$. For $\phi=0$ this is purely Andreev reflection, identical to the one described by Eq. (17), which implies that in this case the interferometer works as a single ideal superconductor–normal-metal (SN) interface. In the general case, $\phi\neq 0$, the reflection consists of both Andreev and normal reflections, the probability of Andreev reflection being given by the matrix element $|(V_n^L)_{11}|^{-2}\sim\cos^2(\phi/2)$. Thus, at $\phi=\pi$ the probability turns to zero, and therefore the Andreev transport through the interferometer is blocked. Furthermore, the transfer matrix $\hat{V}_n^L$ contains information about Andreev bound states in the interferometer. Assuming for a moment the SNS junction disconnected from the injection lead, $T=0$, and considering a stationary version of Eq. (21), $\hat{\alpha}_n^+ = \hat{V}_n^L\hat{\gamma}_n^+$, in combination with Eq. (16) we get the solvability condition for these equations in the form $\mathrm{Im}[(V_n^L)_{11} - (V_n^L)_{12}]=0$, which gives the Andreev level in Eq. (1).

In principle, Eqs. (17), (21), and (15) provide a complete set of recurrences for the MAR amplitudes. However, following Ref. 23, it is convenient to introduce new amplitudes, $\hat{c}_{n\pm}$, which allow us to get rid of redundant MAR amplitudes and to unify notation for different injection cases,

$$\hat{c}_{2m+} = \hat{\alpha}_{2m}^+\delta_{-1\nu} + \hat{\gamma}_{2m}'\delta_{1\nu},$$

$$\hat{c}_{(2m+1)+} = \hat{\gamma}_{2m+1}'\delta_{-1\nu} + \hat{\alpha}_{2m+1}^+\delta_{1\nu},$$

$$\hat{c}_{2m-} = \hat{\gamma}_{2m-1}^+\delta_{-1\nu} + \hat{\alpha}_{2m-1}'\delta_{1\nu},$$

$$\hat{c}_{(2m+1)-} = \hat{\alpha}_{2m}'\delta_{-1\nu} + \hat{\gamma}_{2m}^+\delta_{1\nu}. \tag{24}$$

Then the recurrence relations Eq. (17), (21) and (15) can be written in a compact form

$$\hat{c}_{n+} = \hat{U}_n\hat{c}_{n-} + \hat{Y}_j\delta_{0n}, \tag{25}$$

$$\hat{c}_{(n+1)-} = \hat{T}_n\hat{c}_{n+}, \tag{26}$$

where

$$\hat{U}_n = \delta_{1\mu}\hat{V}_n^R + \delta_{-1\mu}\hat{V}_n^L, \tag{27}$$

$$\hat{T}_n = \frac{1}{\sqrt{2T}}(1-\mu|r_0|\sigma_x), \tag{28}$$

and the index $\mu=(-1)^n\nu$ specifies the particular form of the transfer matrices $\hat{U}_n$ and $\hat{T}_n$ for different sidebands and for different injection directions.

Equations (24)–(28) realize a mapping of the MAR problem on the problem of wave propagation along the energy axis. The wave amplitudes for the propagation in the upward

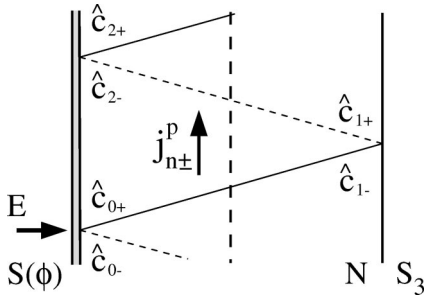

FIG. 3. Schematic picture of the MAR ladder in energy space, for an injected quasiparticle at energy E. The interfaces of the junction are shown as vertical lines, where at the right side there is an ordinary NS interface, while at the left side (double line) there is the effective phase-dependent SN interface. The effective scatterer is shown as a dashed line in the center of the junction. The two-component scattering amplitudes $\hat{c}_{n\pm}$ represent up- and down-going electrons (solid lines) and holes (dashed lines). The corresponding probability current at level n is $j^p_{n\pm}$.

and downward directions are given by the upper, $c^{\uparrow}_{n\pm}$, and lower, $c^{\downarrow}_{n\pm}$, components of the vector $\hat{c}_{n\pm}$,

$$\hat{c}_{n\pm}=\begin{pmatrix} c^{\uparrow}_{n\pm} \\ c^{\downarrow}_{n\pm} \end{pmatrix}. \tag{29}$$

The probability current flowing along the energy axis is defined in the usual way as

$$j^p_{n\pm}=|c^{\uparrow}_{n\pm}|^2-|c^{\downarrow}_{n\pm}|^2. \tag{30}$$

This probability current is conserved within the superconducting gap, $j^p_{n\pm}=\text{const}$ for $|E_n|<\Delta$, due to the unitarity properties of the matrices $\hat{T}_n$ and $\hat{U}_n$. Violation of the unitarity for $\hat{U}_n$ outside the gap indicates leakage of the probability current into the reservoirs. We notice that in real space, the probability current is carried alternatively by electrons and holes, see Fig. 3.

The charge current through the interferometer is determined by the probability currents of all the sidebands,

$$I=\frac{e}{2\pi}\sum_{\nu}\int_{|E|>\Delta} dE \;\; J_{\nu}(E)n_F(E), \tag{31}$$

$$J_{\nu}(E)=\frac{|E|}{\xi}\sum_{j,n=\text{even}}(j^p_{n-}+j^p_{n+}). \tag{32}$$

In this equation, the spectral current $J_{\nu}(E)$ consists of the sum over the scattering states and all the sidebands at the injection side of the junction, ν; the factor $|E|/\xi$ is the superconducting density of states, and $n_F(E)$ is the Fermi distribution function within the superconducting reservoirs.

For $n>0$, the free solution of Eqs. (25) and (26) can be written in the form

$$\hat{c}_{n-}=\hat{M}_{n0}\hat{c}_{0+}, \quad \hat{c}_{n+}=\hat{U}_n\hat{c}_{n-},$$

$$\hat{M}_{n0}=\hat{T}_{n-1}\hat{U}_{n-1}\hat{T}_{n-2}\ldots\hat{U}_1\hat{T}_0, \tag{33}$$

while the solution for negative $n, n<0$, reads

$$\hat{c}_{n+}=\hat{M}^{-1}_{n0}\hat{c}_{0-}, \quad \hat{c}_{n-}=\hat{U}^{-1}_{n}\hat{c}_{n+}.$$

At the injection point $n=0$, the MAR coefficients are found from Eq. (25),

$$\hat{c}_{0+}=\hat{U}_0\hat{c}_{0-}+\hat{Y}_j. \tag{34}$$

This equation imposes two relations between the four unknown coefficients, $c^{\uparrow}_{0\pm}$, $c^{\downarrow}_{0\pm}$; another two relations are imposed by the boundary conditions at infinity in energy space,

$$\lim_{n\to\pm\infty}\hat{c}_{n\pm}=0, \tag{35}$$

which fix the ratios $c^{\uparrow}_{0\pm}/c^{\downarrow}_{0\pm}$. To implement the boundary conditions, we introduce effective reflection coefficients, $r_{n\pm}$, which characterize the intensity of the back scattering at specific points of the MAR ladder. The definition reads

$$\hat{c}_{n+}=c^{\uparrow}_{n+}\hat{r}_{n+} \qquad n\geqslant 0,$$

$$\hat{c}_{n-}=c^{\downarrow}_{n}i\sigma_y\hat{r}_{n-} \qquad n\leqslant 0, \tag{36}$$

where

$$\hat{r}_{n+}=\begin{pmatrix} 1 \\ r_{n+} \end{pmatrix}, \quad \hat{r}_{n-}=\begin{pmatrix} 1 \\ -r_{n-} \end{pmatrix}. \tag{37}$$

With help of the vectors $\hat{r}_{n\pm}$ the solution in Eq. (33) can be presented in a compact form [using the equality $\det(\hat{M}_{nm})=1$],

$$\hat{c}_{n+}=\frac{(\hat{r}^*_{0-},\hat{U}^{-1}_0\hat{Y}_j)}{z_{n0}}\;\hat{r}_{n+} \qquad n>0, \tag{38}$$

where the brackets denote a scalar product of two-component vectors, and

$$z_{n0}=(\hat{r}^*_{0-},\hat{U}^{-1}_0\hat{M}^{-1}_{n0}\hat{U}^{-1}_n\hat{r}_{n+}). \tag{39}$$

The corresponding expression for negative n is

$$\hat{c}_{n-}=-\frac{(\hat{r}^*_{0+},\sigma_y\hat{Y}_j)}{\tilde{z}_{0n}}\sigma_y\hat{r}_{n-} \qquad n<0, \tag{40}$$

$$\tilde{z}_{0n}=(\hat{r}^*_{0+},\sigma_y\hat{U}_0\hat{M}_{0n}\hat{U}_n\sigma_y\hat{r}_{n-}).$$

The form of solution in Eqs. (38)–(40) is particularly useful for the calculation of the SGS: The essential processes which contribute to the SGS involve transmission through the energy-gap region. This transmission contains resonances which are included in the transfer matrix $\hat{M}_{n0}$. The latter is straightforward to calculate because it does not require excursions to infinity. On the other hand, the calculation of the quantities $r_{n\pm}$ includes such excursions which, however, go outside the energy-gap, and the corresponding recurrences rapidly converge.

To calculate the SGS, it is convenient to separate out the current associated with the scattering across the gap, which is

most important for the SGS, from the current of thermal excitations which involves transitions between states below or above the gap. To this end, we first rewrite the spectral current in Eq. (32) through leakage currents into the electrodes defined as $j_n = j^p_{n+} - j^p_{n-}$. By using the equality $j^p_{(n+1)-} = j^p_{n+}$ following from Eq. (26), we get

$$J_\nu(E) = \frac{|E|}{\xi} \sum_{n,j\in\nu} n\, j_{n,j} \tag{41}$$

[here we explicitly write the scattering state index j, introduced in Eq. (4)]. We note that the conservation of the probability current inside the energy gap implies that the leakage current is zero inside the gap, $j_{n,j}=0$, $|E_n|<\Delta$. Having made this observation, we write the total current in Eq. (32) in the form

$$I = \frac{e}{2\pi} \sum_{j,n=1}^{\infty} \int_{-\infty}^{-\Delta} \frac{dE|E|}{\xi}\; n[-j_{-n,j} + \theta(-\Delta - E_n)\, j_{n,j} + \theta(E_n - \Delta)\, j_{n,j}] \tanh\frac{E}{2k_BT}. \tag{42}$$

The first two terms in this equation correspond to the current of thermal excitations: they cancel each other when the temperature approaches zero due to detailed balance,[23]

$$J_{n,\nu}(E) = J_{-n,\mu}(E_n), \tag{43}$$

for the partial currents defined as

$$J_{n,\nu}(E) = n\; \frac{|E|}{\xi} \sum_{j\in\nu} j_{n,j}. \tag{44}$$

Keeping the last term in Eq. (42), we get for the current at low temperature, $T \ll \Delta$, the following equation,

$$I = \sum_{n>0} \theta(eVn - 2\Delta)(I^R_n + I^L_n), \tag{45}$$

$$I^\nu_n = \frac{e}{2\pi} \int_{\Delta - neV}^{-\Delta} dE J_{n,\nu}(E) \tanh\left(\frac{E}{2k_BT}\right). \tag{46}$$

The current $J_{n,\nu}(E)$ in Eq. (44) can be presented after some algebra in the form which is useful for analytical study,

$$J_{n,\nu}(E) = n\; \frac{i_{0,\nu}(E) i_{n,\mu}(E)}{|z_{n0}|^2}, \tag{47}$$

where

$$i_{0,\nu}(E) = (\hat{r}_{0-}[\hat{U}^{*-1}_0 \sigma_z \hat{U}^{-1}_0 - \sigma_z]\hat{r}_{0-}),$$
$$i_{n,\nu}(E) = (\hat{r}_{n+}[\hat{U}^{\dagger -1}_n \sigma_z \hat{U}^{-1}_n - \sigma_z] r_{n+}). \tag{48}$$

III. NUMERICAL CURRENT-VOLTAGE CHARACTERISTICS

In this section, we present the results of numerical calculation of the current given by Eq. (45), where the spectral current is given by Eq. (47). In order to numerically evaluate the effective reflection amplitudes $r_{n\pm}$ we use the following equations,

$$r_{n+} = \lim_{m\to\infty} \frac{M^{\dagger(22)}_{mn}}{M^{\dagger(21)}_{mn}}, \qquad r_{0-} = \lim_{m\to-\infty} \frac{M^{(12)}_{0m}}{M^{(11)}_{0m}}, \tag{49}$$

which follow from the definitions in Eq. (36), using Eq. (33) and Eq. (35). For zero phase difference, the current-voltage characteristic (IVC) in Fig. 4 shows the well-known subharmonic gap structure for short junctions with current structures at $eV = 2\Delta/n$, corresponding to thresholds for the n-particle currents.[27,13] These current structures are associated with the usual gap edge singularities,[23] and they are most pronounced if the transparency $2T$ of the junction is small, $T \ll 1$.

The IVC's of the interferometer for different values of the phase difference at zero temperature are shown in Fig. 5. Increasing the phase difference, the structure changes and the positions of the current structures can no longer be asso-

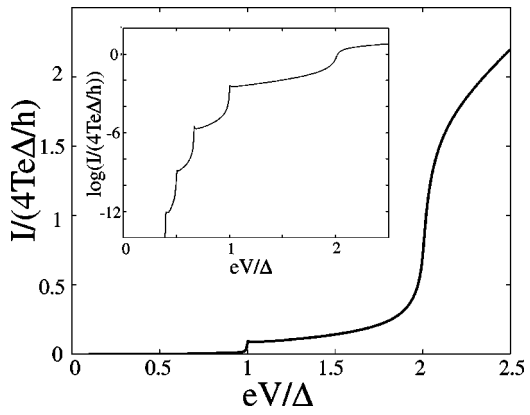

FIG. 4. The subharmonic gap structure of a superconducting point contact with current steps $eV = 2\Delta/n$, $n = 1,2,3,\ldots$ (most visible on the logarithmic diagram). The transmission probability of the point contact is $T_{PC} = 0.08$, which corresponds to an SNS interferometer with $\phi = 0$ and $2T = 0.08$.

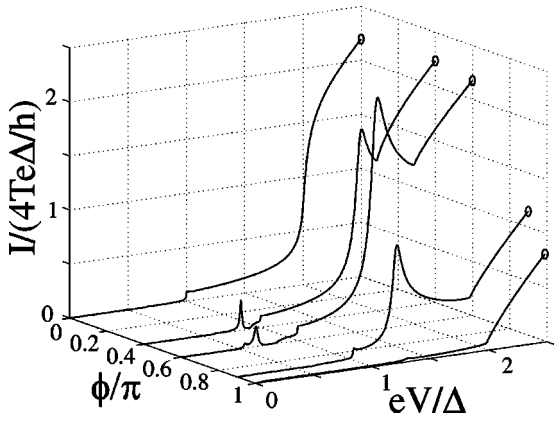

FIG. 5. The current-voltage characteristics at zero temperature of an interferometer with $2T = 0.08$, $R = 0.1$, and $\phi = 0, \phi = 2\pi/5, \phi = 3\pi/5, \phi = 0.9\pi$, and $\phi = 0.99\pi$.

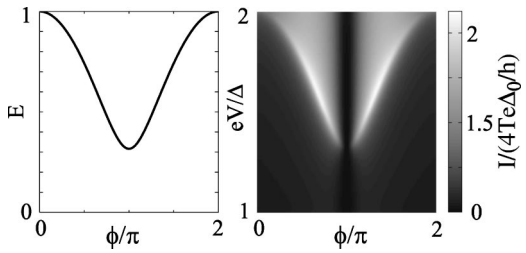

FIG. 6. Left: the energy of the (positive) Andreev level for $D=0.9$, as a function of the phase difference. Right: the current peak (light region) at $eV \approx \Delta + E_a(\phi)$ follows the position of the Andreev level.

ciated with the subharmonics of the energy-gap. Instead, we observe enhancement of the subgap current and the appearance of large current peaks which move downwards in voltage with an increasing phase difference. If the transparency is small, as in Fig. 5, the peak positions reflect the Andreev spectrum of Eq. (1): the peaks appear at $eV \approx E_a$ and $eV \approx \Delta + E_a$, as shown in Fig. 6. With further increase of the phase difference, the current structures decrease and completely disappear at $\phi = \pi$. At the same time, the excess current at large voltage becomes large and negative, turning into a deficit current. The IVC is 2π periodic and symmetric around π.

It is illuminating to plot the individual n-particle currents, given by Eq. (46). In Fig. 7, the first four n-particle currents are shown for $\phi = 3\pi/5$ and for the same interferometer parameters as in Fig. 5. Higher-order currents are too small to be visible in the same picture, and their contribution to the current may be neglected. For comparison, the inset shows the corresponding IVC's when $\phi = 0$. It follows from the plots for $\phi \neq 0$ that the peak at low voltage originates exclusively from the four-particle current. It exists within the voltage interval $\Delta/2 < eV < \Delta$ and within a certain window of

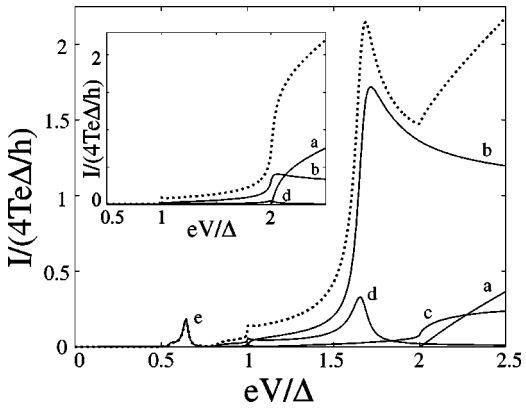

FIG. 7. The current-voltage characteristics of the same interferometer as in Fig. 5 with $\phi = 3\pi/5$. The total current is shown with the dotted line. The single-particle current (a) is suppressed compared to the case when $\phi = 0$. The two-particle current (b) of quasiparticles injected from the right electrode has a significant onset at $eV = \Delta + E_a$, while the two-particle current (c) injected from the left is small. The three-particle current (d) has a peak at $eV \approx \Delta + E_a$; the four-particle current (e) has a peak at $eV \approx E_a$. The inset shows the corresponding *n*-particle IVC's for $\phi = 0$.

phase difference. The next peak, at larger voltage, results from a combination of two structures: the peak of the three-particle current, and the overshoot of the onset of the pair current. The onset of a single-particle current at $eV > 2\Delta$ is reduced in comparison with the $\phi = 0$ case, which leads to significant reduction of the current at large voltage. The reason is spectral intensity transfer from the continuum to bound Andreev states. The large deficit current at high voltage is apparently the result of this reduction as well as of the above-mentioned reduction of the multiparticle currents related to the suppression of Andreev reflections by the interferometer. The further analysis shows that the single- and three-particle currents (and in general odd *n*-particle currents) injected from the electrode S_3 and from the electrodes $S_{1,2}$ are identical. In contrast, the two- and four-particle currents possess large structures only for injection from the electrode S_3 while currents injected from the interferometer electrodes $S_{1,2}$ are negligibly small. In the next section, we will proceed with the interpretation of these features.

IV. RESONANCE APPROXIMATION

In the case of weak coupling of the S_1NS_2 junction in the interferometer to the injection lead $S_3, T \ll 1$, it is possible to perform a perturbative analysis of the *n*-particle currents in order to explain the origin of the phase-dependent current structures in the IVC's. In this limit, the current is dominated by the contribution of the Andreev resonances, which we will consider in the lowest order with respect to the small parameter $T \ll 1$. We will proceed with a detailed analysis of the four lowest-order *n*-particle currents in order to explain the major structures in the current-voltage characteristics (IVC).

Let us start the discussion with the approximation for the effective reflection amplitudes at specific levels in the MAR ladder, $\hat{r}_{n\pm}$, in Eq. (37). In the lowest-order approximation with respect to *T*, these reflection amplitudes are contributed by single backscattering,

$$\hat{r}_{n\pm} = \begin{pmatrix} 1 \\ \mp \nu(-1)^n r_0 \end{pmatrix} + O(T^2). \tag{50}$$

Since the denominator $|z_{n0}|^2$ in Eq. (47) for the spectral current contains a factor $1/(2T)^n$ which comes from the product of transfer matrices $\hat{T}_n$ in Eq. (33), we can neglect all terms except the zero-order one in Eq. (48), whereby

$$i_{n,\mu} = i_n^L \delta_{-1,\mu} + i_n^R \delta_{1,\mu} \qquad n > 0,$$

$$i_n^L = \frac{4|E_n|}{\Delta^2} \frac{(E_n^2 - E_a^2)}{\xi_n \cos^2 \dfrac{\phi}{2}}, \qquad i_n^R = \frac{4|E_n|\xi_n}{\Delta^2}. \tag{51}$$

The denominator $|z_{n0}|^2$ in Eq. (47) has to be considered separately for different currents, *n*, and injection cases, ν.

The single-particle current involves only a single crossing of the tunnel barrier, schematically shown in Fig. 9(a) below. Thus, it cannot be resonant, and the denominator $|z_{10}|^2$ can be considered in the lowest-order approximation. The ex-

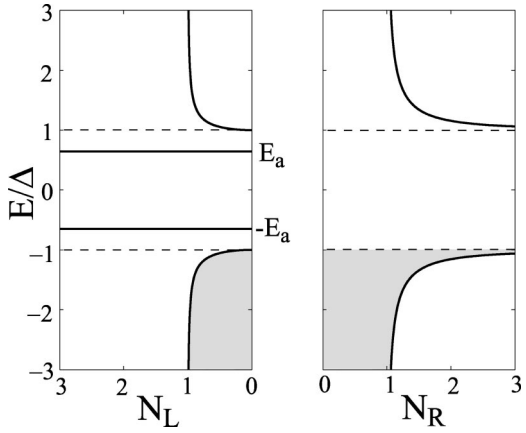

FIG. 8. The effective superconducting density of states in the left and the right electrodes of the SNS interferometer, with $D=0.9$ and $\phi=3\pi/5$. The shaded regions represent the states filled at zero temperature. When the phase difference is changed from zero, the bound Andreev states split from the continuum, and the peaks in the density of states at the gap edges are smeared in the left electrode.

pression for the single-particle current, derived from Eqs. (46), (47), and (51) then reads

$$I_1=\frac{2Te}{\pi}\int_{\Delta-eV}^{-\Delta} dE\ \ N_L(E)N_R(E+eV), \tag{52}$$

where

$$N_L(E)=\frac{|E|\sqrt{E^2-\Delta^2}}{E^2-E_a^2}, \tag{53}$$

$$N_R(E)=\frac{|E|}{\sqrt{E^2-\Delta^2}}. \tag{54}$$

The form of Eq. (52) is a standard one for a tunnel current given by the tunnel Hamiltonian model where $N_R(E)$ is the density of states (DOS) in the injection lead, while $N_L(E)$ has the meaning of the effective phase-dependent DOS in the interferometer. An important property of the DOS of the interferometer is the disappearance of the singularities at the gap edges for a nonzero phase difference. The reason is that the resonances (Andreev states) move down into the gap, according to Eq. (1) (see Fig. 8). Consequently, the onset of the single-particle current at $eV=2\Delta$, which is of the order T when $\phi=0$, is reduced at a finite phase difference (see Fig. 7).

In order to calculate the pair current we will first inspect the corresponding transfer matrix, $\hat{M}_{20}^{-1}=\hat{T}_0^{-1}\hat{U}_1^{-1}\hat{T}_1^{-1}$. For $\nu=1$ (injection from the right) this transfer matrix has zeros in the limit $T=0$ at the energies of the Andreev bound states in the interferometer, $E_1=\pm E_a$. The expansion of the matrix in powers of T has the form

$$\hat{M}_{20}^{-1}=\frac{1}{T|\xi_1|\cos\frac{\phi}{2}}\Bigg[(E_1^2-E_a^2)(\sigma_z-i\sigma_y)(1-T)$$

$$+iT\left(E_1|\xi_1|-\sigma_x\sqrt{DR}\sin^2\frac{\phi}{2}\right)\Bigg]+O(T^2), \tag{55}$$

where we have used the identity, $\sin\theta=2\sqrt{DR}$, derived from the unitarity condition Eq. (11) and $\theta=\theta'+\rho$, in the limit $T=0$. Equation (55) clearly demonstrates the resonant behavior. The first term is real and proportional to the deviation of the energy E_1 for the Andreev reflection from the energy of the Andreev state. This term determines the position of the resonance. The second, imaginary term is proportional to T and determines the width of the resonance. Both the position and width of the resonance depend on the phase difference. At $T\ll 1$ the spectral current is dominated by the Andreev resonance, and neglecting the nonresonant current we arrive at the expression

$$I_2^R=\frac{2e}{\pi}\int_{\Delta-eV}^{eV-\Delta} dE_1\frac{\Gamma_+\Gamma_-}{(E_1-E_a)^2+\left(\frac{\Gamma_++\Gamma_-}{2}\right)^2}, \tag{56}$$

where

$$\Gamma_\pm=TD_\pm N_R(E_a\mp eV), \tag{57}$$

$$D_\pm=\frac{1}{2}\left(\sqrt{\Delta^2-E_a^2}\pm\frac{\sqrt{DR}\Delta^2}{E_a}\sin^2\frac{\phi}{2}\right), \tag{58}$$

$0\leqslant D_\pm\leqslant\sqrt{D}$. A factor of 2 appears in the current expression, in addition to the two-particle factor $n=2$ in Eq. (47), since there are two Andreev resonances, at E_a and $-E_a$. The integrand in Eq. (56) has the form of the transmission coefficient for an asymmetric quantum-mechanical double barrier structure. The difference in the tunnel rates $\Gamma_\pm$ is due to the different DOS for the injection and exit energies, but also due to the different effective transparencies of the Y-branch splitter, $TD_\pm$, for electrons and holes. The resonant transparency of the junction for the pair current is proportional, according to Eq. (56), to the product

$$D_+D_-=\frac{\Delta^2(\Delta^2-E_a^2)}{4E_a^2}\cos^2\frac{\phi}{2}, \tag{59}$$

which turns to zero at $\phi=\pi$. Thus the resonant pair current is blocked at $\phi=\pi$, in agreement with our earlier general conclusion about the suppression of Andreev reflection at the interferometer in this case. Evaluation of the integral over energy in Eq. (56) under the condition, $E_a/\Delta<1-T$, yields the pair current

$$I_2^R=\frac{4e\Gamma_+\Gamma_-}{|\Gamma_++\Gamma_-|}. \tag{60}$$

The magnitude of this current is generally of order T; however, in the vicinity of the resonant onset, $eV=\Delta+E_a+e\,\delta V$ for deviations $e\,\delta V$, the rate Γ_+ increases due to the enhancement of the DOS in the right superconductor, Γ_+

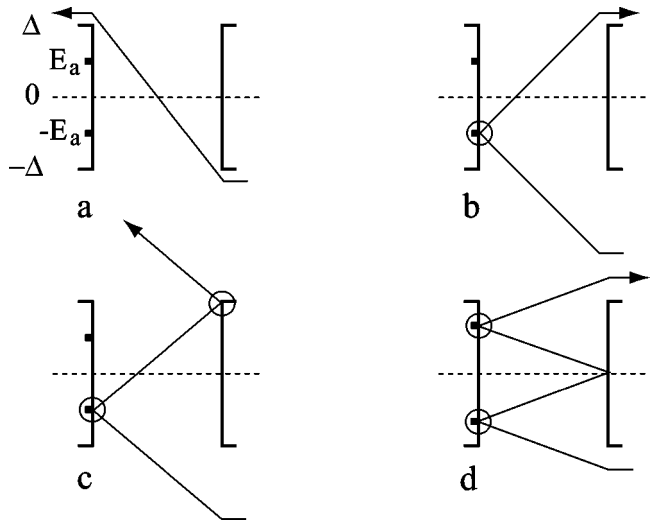

FIG. 9. Schematic pictures of important scattering processes. Resonances are shown as circles. (a): Nonresonant single-particle current; (b): resonant pair current from the right side involves one resonant Andreev reflection, and two equivalent resonant paths are possible; (c): resonant three-particle current involves one resonant Andreev reflection and one reflection by the quasiresonance at the energy-gap edge. An equivalent path exists also for injection from the left; (d): resonant four-particle current involves two resonant Andreev reflections (double resonance).

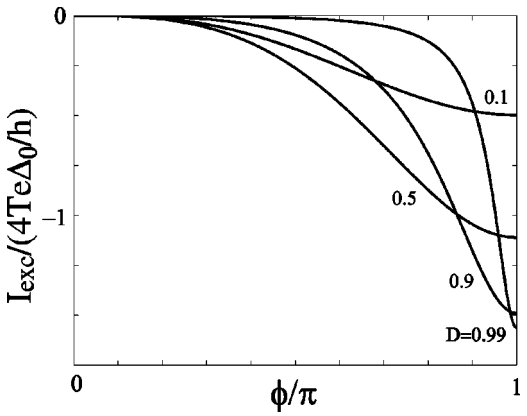

FIG. 10. The first-order ($\sim T$) excess current as a function of the phase difference for different transparencies D of the SNS junction of the interferometer.

$\sim 1/\sqrt{\delta V}$, which yields the overshoot seen in Fig. 7. At lower voltage, $\Delta < eV < \Delta + E_a$, the pair current is nonresonant and proportional to T^2, which is also the case for the pair current I_2^L injected from the interferometer.

The resonant three-particle current can be analyzed in a similar manner. We construct the corresponding transfer matrix using the pair current matrix, Eq. (55), and for $\nu = 1$ we get $\hat{M}_{30}^{-1} = \hat{M}_{20}^{-1} \hat{U}_2^{-1} \hat{T}_2^{-1}$. This equation has resonances at the same energies as the pair current, $E_1 = \pm E_a$, but nevertheless the resonant current is small, $I_3 \sim T^2$, since the MAR path, Fig. 9(c), includes an additional crossing of the tunnel barrier. The magnitude of the current is considerably enhanced in the vicinity of voltage $eV = E_a + \Delta$ when the second Andreev reflection occurs at the gap edge of the right electrode, $E_2 = \Delta$ [see Fig. 9(c)]. The singular DOS at the gap edge in this electrode appears in the MAR calculation as a quasibound state situated at the gap edge. Thus, this MAR process can be interpreted as an overlap of two resonances, one at the Andreev bound state at energy $-E_a$, and another at the quasibound state at the gap edge. A similar analysis applies to the current injected from the interferometer, $\nu = -1$: in this case, the double resonance is formed by the Andreev state at E_a and the quasibound state at the lower gap edge. The height of the double-resonance peak is $(I_3)_{max} \sim T^{4/3}$.

A double resonance involving two Andreev bound states occurs in the four-particle current injected from the right as shown in Fig. 9(d). The corresponding MAR path is selected by the conditions $E_1 = -E_a$ and $E_3 = E_a$. The resulting peak is situated at $eV = E_a$ and has the height $(I_4)_{max} \sim T$. In the vicinity of the peak, $e\delta V = eV - E_a \ll \Delta$, the expression for the resonant four-particle current becomes

$$I_4^R = \frac{e}{2\pi} \int_{-\infty}^{\infty} \frac{dE_2 \tilde{\Gamma}_-^2 \Gamma_0^2}{\left[E_2^2 - (e\delta V)^2 - \frac{1}{4}(\tilde{\Gamma}_-^2 + \Gamma_0^2) \right]^2 + E_2^2 \tilde{\Gamma}_-^2}, \tag{61}$$

where

$$\Gamma_0 = TD_+, \quad \tilde{\Gamma}_- = TD_- N_R(2E_a). \tag{62}$$

The current peak under consideration is a full-scale current structure in a region of the IVC that in point contacts is dominated by a nonresonant four-particle current, which is of the order T^4. As any Andreev resonance, the four-particle current peak strongly depends on the phase difference; it disappears at $\phi = \pi$. The peak exists within the voltage interval $\Delta/2 < eV < \Delta$ and within the phase difference window $0 < \sin^2\phi/2 < 3/(4D)$. We note that the positions of all discussed current structures are proportional to the order parameter Δ and therefore temperature dependent and scale with Δ.

We end this section with the discussion of IVC's at large voltage, $eV \gg 2\Delta$. The current at large voltage results exclusively from the single-particle and pair currents. It is straightforward to calculate the single-particle current at large voltage from Eq. (52),

$$I_1 = \frac{2T}{\pi} \int_{\Delta}^{eV-\Delta} \frac{dE_1 E_1 \xi_1 E_0}{(E_a^2 - E_1^2)\xi_0} = \frac{2Te^2V}{\pi} + I_{1,exc}. \tag{63}$$

The first term in this equation is the current through the normal junction, while the second term is the single-particle contribution to the excess current,

$$I_{1,exc} = -eT\sqrt{D}\Delta |\sin(\phi/2)| + O(T^2). \tag{64}$$

This excess current is large, $\sim T$, and negative, which reflects the suppression of the current onset at $eV = 2\Delta$. The pair current contribution to the excess current is dominated by the

resonance and is given by Eq. (60). The total excess current to leading order in T has the form

$$I_{exc} = -eT\Delta\sqrt{D}R\frac{|\sin(\phi/2)|^3}{1-D\sin^2(\phi/2)}. \quad (65)$$

The excess current in the interferometer is large and negative, in sharp contrast to quantum point contacts, where the excess current is small, $\sim T^2$, and positive.[22] However, it turns to zero at $\phi=0$, in agreement with our observation that in this case the interferometer behaves as a quantum point contact. The excess current achieves its minimum value at $\phi=\pi$ because of a blockade of the pair current, see Fig. 10.

V. CONCLUSIONS

We have investigated the phase dependence of the dc CVC's in SNS interferometers consisting of two superconducting reservoirs connected by a Y-shaped normally conducting quantum wire. We have developed a generalization of the existing coherent MAR theory, which fully incorporates the effect of interference, as well as resonance effects due to Andreev bound states in the interferometer.

The phase-dependent current-voltage characteristic $I(V,\phi)$ has been numerically investigated for single-mode wires with lengths smaller than the superconducting coherence length. The analytical study of the current was performed using a resonance approximation in the limit of weak coupling of the interferometer to the injection lead.

We found significant enhancement of the subgap current at a finite phase difference compared to the case of a zero phase difference. The enhancement is accompanied by a shift of the onset of the current at 2Δ to smaller voltages, $\Delta+E_a(\phi)<2\Delta$, and the appearance of current peaks at E_a and $\Delta+E_a$. These features are produced by resonant Andreev reflection of the injected particles by the S_1NS_2 junction of the interferometer: they are most pronounced for weak coupling of the S_1NS_2 junction to the injection lead. The positions of all current structures are temperature dependent and scale with Δ.

We further found strong suppression of the current when the phase difference approaches $\phi\to\pi$: in this region all subgap current structures disappear and, moreover, the excess current at large voltage becomes negative (deficiency current). The magnitude of the deficiency current is considerably large at $\phi=\pi$. This effect results from the suppression of the Andreev reflections from the S_1N and S_2N interfaces due to the interference in the arms of the beam splitter (cf. a similar effect in NS interferometers[5,6]).

We conclude our discussion with some brief comments on the connection of the studied model to more realistic experimental devices based on 2D electron-gas structures. In such devices, the normal region has a typical size which exceeds the superconducting coherence length and it contains several conducting electronic modes. Furthermore, the NS interfaces are not perfectly transparent. However, this effect is less important since the interface reflection coefficient in practice can be rather small (<0.2). Increasing the length of the arms of the interferometer will result in the appearance of new phase-dependent current peaks due to the increasing number of Andreev states in the SNS junction of the interferometer (cf. Ref. 19). Similarly, increasing the length of the injection lead will result in the appearance of current resonances which do not depend on the phase difference, due to ϕ-independent superconducting bound states in this lead.[14] In interferometers with multimode wires, the resonant current peaks will be smeared; however, one should still expect some phase-dependent resonant features similar to the case of diffusive NS interferometers.[6] The interference effect leading to the large deficient current at large applied voltage will survive in multimode junctions.

ACKNOWLEDGMENTS

The authors gratefully acknowledge support from NFR and KVA (Sweden) and NEDO (Japan).

[1] Th. Martin and R. Landauer, Phys. Rev. B **45**, 1742 (1992).
[2] M. Büttiker, Phys. Rev. B **46**, 12 485 (1992).
[3] R.C. Liu, B. Odom, Y. Yamamoto, and S. Tarucha, Nature (London) **391**, 263 (1998).
[4] J. Torrés and Th. Martin, Eur. Phys. J. B **12**, 319 (1999).
[5] H. Nakano and H. Takayanagi, Phys. Rev. B **47**, 7986 (1993).
[6] F.W.J. Hekking and Yu.V. Nazarov, Phys. Rev. Lett. **71**, 1625 (1993).
[7] A.F. Andreev, Zh. Éksp. Teor. Fiz. **46**, 1823 (1964) [Sov. Phys. JETP **19**, 1228 (1964)].
[8] V.T. Petrashov, V.N. Antonov, P. Delsing, and R. Claeson, Phys. Rev. Lett. **70**, 347 (1993).
[9] P.G.N. de Vegvar, T.A. Fulton, W.H. Mallison, and R.E. Miller, Phys. Rev. Lett. **73**, 1416 (1994).
[10] C.J. Lambert and R. Raimondi, J. Phys.: Condens. Matter **10**, 901 (1998).
[11] T.M. Klapwijk, G.E. Blonder, and M. Tinkham, Physica B & C **109-110**, 1657 (1982).
[12] J.M. Rowell and W.L. Feldmann, Phys. Rev. **172**, 393 (1968).
[13] E.N. Bratus', V.S. Shumeiko, and G. Wendin, Phys. Rev. Lett. **74**, 2110 (1995).
[14] Å. Ingerman, G. Johansson, V.S. Shumeiko, and G. Wendin, Phys. Rev. B **64**, 144504 (2001).
[15] A phase-dependent single-particle tunnel current in four-terminal superconductor–insulator–normal-metal–superconductor interferometers with diffusive normal regions was recently studied in F.K. Wilhelm and A.A. Golubov, Phys. Rev. B **62**, 5353 (2000).
[16] J. Kutchinsky, R. Taboryski, O. Kuhn, C.B. Sørensen, P.E. Lindelof, A. Kristensen, J. Bindslev Hansen, C. Schelde Jacobsen, and J.L. Skov, Phys. Rev. B **56**, R2932 (1997).
[17] H. Takayanagi, E. Toyoda, and T. Akazaki, Superlattices Microstruct. **25**, 993 (1999).
[18] A. Kadigrobov, A. Zagoskin, R.I. Shekhter, and M. Jonson, Phys. Rev. B **52**, R8662 (1995).
[19] P. Samuelsson, V.S. Shumeiko, and G. Wendin, Phys. Rev. B **56**, R5763 (1997); **62**, 1319 (2000).

[20] L.F. Chang and P.F. Bagwell, Phys. Rev. B **55**, 12 678 (1997).
[21] D. Averin and A. Bardas, Phys. Rev. Lett. **75**, 1831 (1995).
[22] V.S. Shumeiko, E.N. Bratus', and G. Wendin, Low Temp. Phys. **23**, 181 (1997).
[23] G. Johansson, E.N. Bratus', V.S. Shumeiko, and G. Wendin, Superlattices Microstruct. **25**, 905 (1999).
[24] G. Johansson, E. Bratus', V. Shumeiko, and G. Wendin, Phys. Rev. B **60**, 1382 (1999).
[25] P.G. de Gennes and D. Saint-James, Phys. Lett. **4**, 151 (1963).
[26] P.G de Gennes, *Superconductivity in Metals and Alloys* (Addison-Wesley, Reading, MA, 1989).
[27] J.R. Schrieffer and J.W. Wilkins, Phys. Rev. Lett. **10**, 17 (1963).